Accepted Manuscript

Development of least sized magnetic nanoparticles with high saturation magnetization

K. Srinivasa Rao, P. Appa Rao, M. Chaitanya Varma, K.H. Rao

Please cite this article as: K.S. Rao, P.A. Rao, M.C. Varma, K.H. Rao, Development of least sized magnetic nanoparticles with high saturation magnetization, *Journal of Alloys and Compounds* (2018), doi: 10.1016/j.jallcom.2018.04.002.

Development of least sized magnetic nanoparticles with high Saturation magnetization

K. Srinivasa Rao[1]*, P. Appa Rao[2], M. Chaitanya Varma[3], and K. H. Rao[4]

[1]Department of Physics, PBN College, Nidubrolu, 522124, India

[2]Department of Physics, Dadi Institute of Engineering and Technology, Anakapalli, 531002, India

[3]Department of Physics, Institute of Technology, GITAM (Deemed to be University), Visakhapatnam, 530045, India

[4]IIIT, RGUKT, Nuzvid, 521202, India

*corresponding author's email: ksr_gvsk@yahoo.co.in

Abstract

Magnetic nanoparticles of high saturation magnetization with least particle size are essential candidates for certain biomedical applications like hyperthermia. The development of such nanoparticles requires stringent processing conditions in arriving at desired characteristics. Magnesium substituted cobalt ferrite nanoparticles of size around 4 nm were processed by sol-gel method with high saturation magnetization and characterized by techniques XRD, TEM, FESEM and FTIR in elucidating the structural parameters. Magnetic properties were discussed in terms of a proposed cation distribution and occupancy of magnesium was established from electrical resistivity measurements.

Keywords: Cobalt magnesium ferrite, Sol-gel process, Magnetic properties, TEM & FESEM images, DC resistivity

1. Introduction

Cobalt ferrite, a well-studied spinel ferrite for transducer and magnetostrictive [1] sensor applications finds its importance, these days, in the field of biomedicine due to its larger magnetic anisotropy. Cobalt ferrite nanoparticles find their place as enhancement agents for signal reception in magnetic resonance imaging (MRI), and offer better heating absorption capacity for magnetically tagging devices of bio-entities, bio-separation and drug delivery [2, 3]. Recently, cobalt ferrite magnetic nanoparticles are intensively studied for their potential use for magnetic hyperthermia applications where the studies mainly focus on attaining a high specific absorption rate, investigating magnetic hysteresis, obtaining superparamagnetic nanoparticles with high saturation magnetization coupled with low Curie temperatures and producing least sized particles [4, 5]. The extensive applications of cobalt ferrite thus attracted many a researcher for its further developments in varied fields. The performance of the magnetic nanoparticles as a good hyperthermia mediator is dependent on the intensity, frequency of alternating magnetic field and the time of exposure of the tumour which collectively decide the heat generated due to power loss. In turn, the power loss relates to the saturation magnetization of the material and several magnetization reversal processes, which may appreciably vary with the particle size of the nanoparticles.

The processing of cobalt ferrite nanoparticles in relation to size with unique magnetic properties was treated by several researchers by adopting various methods. The sol-gel method was found to yield fine particles [6] of the required size with high saturation magnetization, low particle size, with an inclination towards the occurrence of superparamagnetism.

Toksha et.al. [7] fabricated cobalt ferrite nanoparticles in the range 11-40 nm by sol-gel auto combustion method and reported the highest saturation magnetization, 76emu/g for the particles of size 40 nm. An attempt was made by Jae-Gwang Lee et al. [8] in producing ultra-fine cobalt ferrite particles by the sol-gel method through annealing the dried powder from 200°C to 850°C with maximum values of coercive field (2020 Oe) and the saturation magnetization (76.5 emu/g). The cation distribution of cobalt ferrite nanoparticles synthesized by sol-gel auto combustion method indicates that a major portion of the cobalt (94%) occupies octahedral sites [9]. However, the results of Mossbauer spectroscopy showed that 60% of the cobalt occupied octahedral sites [10].

The saturation magnetization of cobalt ferrite may further be enhanced by incorporating sufficient amounts of diamagnetic ions in place of cobalt. However, the results available are often conflicting with one another. The saturation magnetization of Co-Zn nano ferrite was observed to decrease monotonically with the increasing Zn concentration [11]. On the other hand, the saturation magnetization in $Co_{1-x}Zn_xFe_2O_4$ (x = 0.0, 0.2, 0.4, 0.6, 0.8 and 1.0) showed an increase up to x = 0.4 followed by a decrease at higher concentrations of zinc [12].

Interestingly, there exist very few detailed studies on cobalt ferrites containing another diamagnetic material, magnesium. Magnesium substitution having a stronger preference to occupy octahedral sites is known to control the magnetic properties of ferrite [13]. Substitution of Mg^{2+} ions not only reduces the super-exchange interaction between the ions at A and B sites, but also causes a decrease in Curie temperature and magnetic anisotropy [14]. A decrease in saturation magnetization was noticed with an increase of magnesium content in $Co_{1-x}Mg_xFe_2O_4/SiO_2$ nano composites with a maximum coercive field 2604Oe for x = 0.6 [15] whereas an increase was reported from x = 0.25 to 0.45 in $Co_{1-x}Mg_xFe_2O_4$ [16]. A decrease in both saturation magnetization and coercivity was observed [17] with increasing magnesium content in nano $Mg_xCo_{1-x}Fe_2O_4$ (x = 0, 0.2, 0.4, 0.6, 0.8 and 1.0) ferrite. The decrease in the effective magnetic anisotropy in $Co_{1-x}Mg_xFe_2O_4$ (x = 0.0 – 0.6) was interpreted in terms of cation distribution between the A and B sites by Franco Jr., et al [18]. Further, Mg^{2+} ions were reported to occupy both A and B sites for smaller concentration (x = 0.25) and the B-sites for higher concentrations (x = 0.50 and 0.75) in $Co_{1-x}Mg_xFe_2O_4$ (x = 0.0, 0.25, 0.50, 0.75 and 1.0) system [19]. In another report, Mg^{2+} ions were observed to occupy the only B-sites in nano $Co_{1-x}Mg_xFe_2O_4$ (x = 0.0, 0.2, 0.4, 0.6, 0.8 and 1.0) ferrite [20].

Substitution of diamagnetic elements like zinc, or magnesium in cobalt ferrite is likely to enhance the saturation magnetization by modifying the magnetic anisotropy. The rise in saturation magnetization may further be envisaged if diamagnetic impurity element occupies A-sites at lower concentrations. The reports available in the literature show a scanty picture in understanding the modifications related to magnetization and the influence of chelating agents in controlling the particle size. A thorough knowledge is inevitable about the site

occupancy of various cations over A and B sub-lattices, for producing a suitable material with desired properties. A suitable material for magnetic hyperthermia applications may be developed by optimizing the processing conditions and controlling the magnetic properties.

The present work describes a systematic study of developing least sized magnesium substituted cobalt ferrite nanoparticles with high saturation magnetization by elucidating their microstructure and cation distribution.

2. Experimental details

Samples with composition, $Co_{1-x}Mg_xFe_2O_4$ varying x from 0.00 to 0.20 in steps of 0.04 (2 mole %) were prepared by the sol-gel method using polyvinyl alcohol as chelating agent. Analytical grade nitrates of cobalt, magnesium and iron were weighed according to the required stoichiometric proportion and dissolved each in a minimum amount of de-ionized water. The formed cationic solutions were mixed and stirred for 2 hours to improve the homogeneity and the resulting solution is known as the precursor. The ratio of ferrite to PVA (chelating agent) was maintained at 1:3 [6].The PVA (10% W/V) solution was prepared by dissolving 10 grams of chelating agent in 100 mL of de-ionized water. A clear polyvinyl alcohol (PVA) solution was added to the precursor and dehydrated around 100 °C under continuous and constant stirring. The gelation continued step by step till a voluminous charred fluffy mass was formed. Later, the mass was dried in a hot air oven for 10 hours to remove any water content that persists in the material. The dried powder was annealed at 400 °C in a furnace under a heating rate of 5 °C/minute for an hour, followed by cooling in air atmosphere by switching the furnace off. A small amount of the powder annealed at 400 °C was made into pellets and toroids using polyvinyl alcohol as a binder before subjecting them to further heat treatment in air for another hour at 1050 °C under the heating rate of 5 °C per minute.

2.1   Characterization

The formation of spinel structure of the $Co_{1-x}Mg_xFe_2O_4$ samples was studied using X-ray Bruker advanced D8 X-ray diffractometer operated at 44 kV and 100 mA. The sample was irradiated with Cu-K$_\alpha$ radiation ($\square$ = 1.5406 Å) and scanned at 0.02 $^\circ$/Sec in the range 5-100°. Lattice parameter has been estimated from the observed Bragg angles, considering Nelson-Riley function to minimize the error in its determination. The infrared spectrum of the samples was recorded at room temperature using the FTIR spectrometer (Perkin Elmer model 1650) in the range 300-4000 cm^{-1} by KBr pellet method. The specific saturation magnetization measurement was made using a vibrating sample magnetometer (Lake Shore 4700) operating at a maximum field of 18 kOe. The temperature dependence of permeability was recorded using 6500 P WAYNE KERR high frequency LCR meter at 100 kHz for all the samples. DC resistivity was estimated by measuring current accurately with the help of digital nanoammeter model DNM-121 using two-probe method. The transmission electron microscope (TEM) images of the nanoparticles were obtained with a JOEL JEM 200CX model electron microscope operated at 120 kV. Sample preparation involves dispersion of a small quantity of ferrite powder in de-ionized water using ultrasonicator. A drop of dispersed liquid is placed on a carbon-coated copper grid using a dropper and dried for at least 24 h at room temperature. The experimental density, obtained for each sample using the Archimedes' principle was compared with the theoretical X-ray density, estimated using the equation $d_x = 8M/Na^3$, where M is the molecular weight of the composition, N is the Avogadro's number and 'a' is the lattice parameter.

3. Results and Discussions
3.1   X-ray diffraction

X-ray diffraction patterns of all the samples (figure 1) confirmed the spinel structure with no impurity phases. Identification of the spinel phase was made with the help of ICDD card number 22-1086.
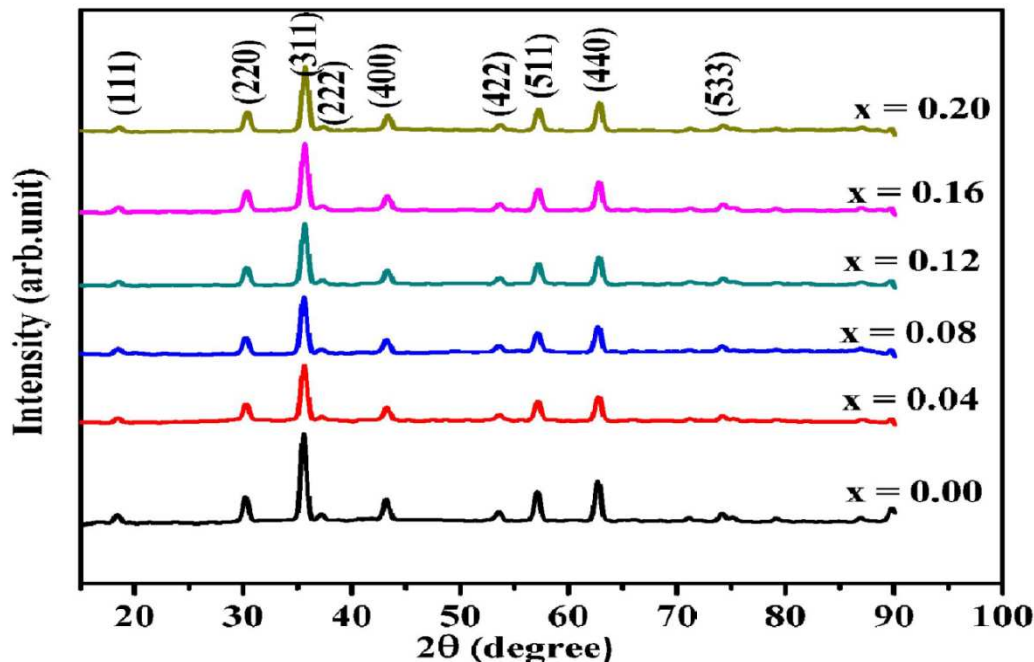

Fig.1 X-ray diffraction patterns of magnesium substituted cobalt ferrite.

The decrease in estimated lattice parameter (table1) with magnesium concentration indicates the accommodation of magnesium ions in the ferrite lattice and the same has been attributed to the small ionic radius of substituted magnesium (0.72 Å) as compared to the displaced Co^{2+} ion (0.745 Å) at B-site [21].

The observed gradual decrease in both bulk and X-ray densities with increasing magnesium concentration has been primarily due to the replacement of cobalt ions of higher atomic weight with magnesium ions of lower atomic weight. On the other hand, the lower density of magnesium/magnesium ferrite as compared to that of cobalt/cobalt ferrite could also be another reason for the observed decrease in density of the magnesium substituted cobalt ferrite system. Further, the smaller difference between the two values of experimental and X-ray densities for each composition may arise due to intergranular porosity of the sample, resulted from the lower melting point of magnesium (650 °C) as compared to that of cobalt (1495 °C).

3.2   Transmission Electron Micrographs

Transmission Electron Micrographs and histograms of all the magnesium substituted cobalt ferrite samples, $Co_{1-x}Mg_xFe_2O_4$ are shown in figure 2. Mean particle size has been estimated from a transmission electron micrograph considering the observed linear size of the particles at different locations using Image J software by fitting the particle size distribution with a Gaussian function. The particle size estimation involves a count of about 200 particles taken from two image pictures of each sample. The images corresponding to x = 0.04 & 0.08

reflect the agglomeration characteristic of the prepared nanoparticles to a certain extent where primary particles are held together.
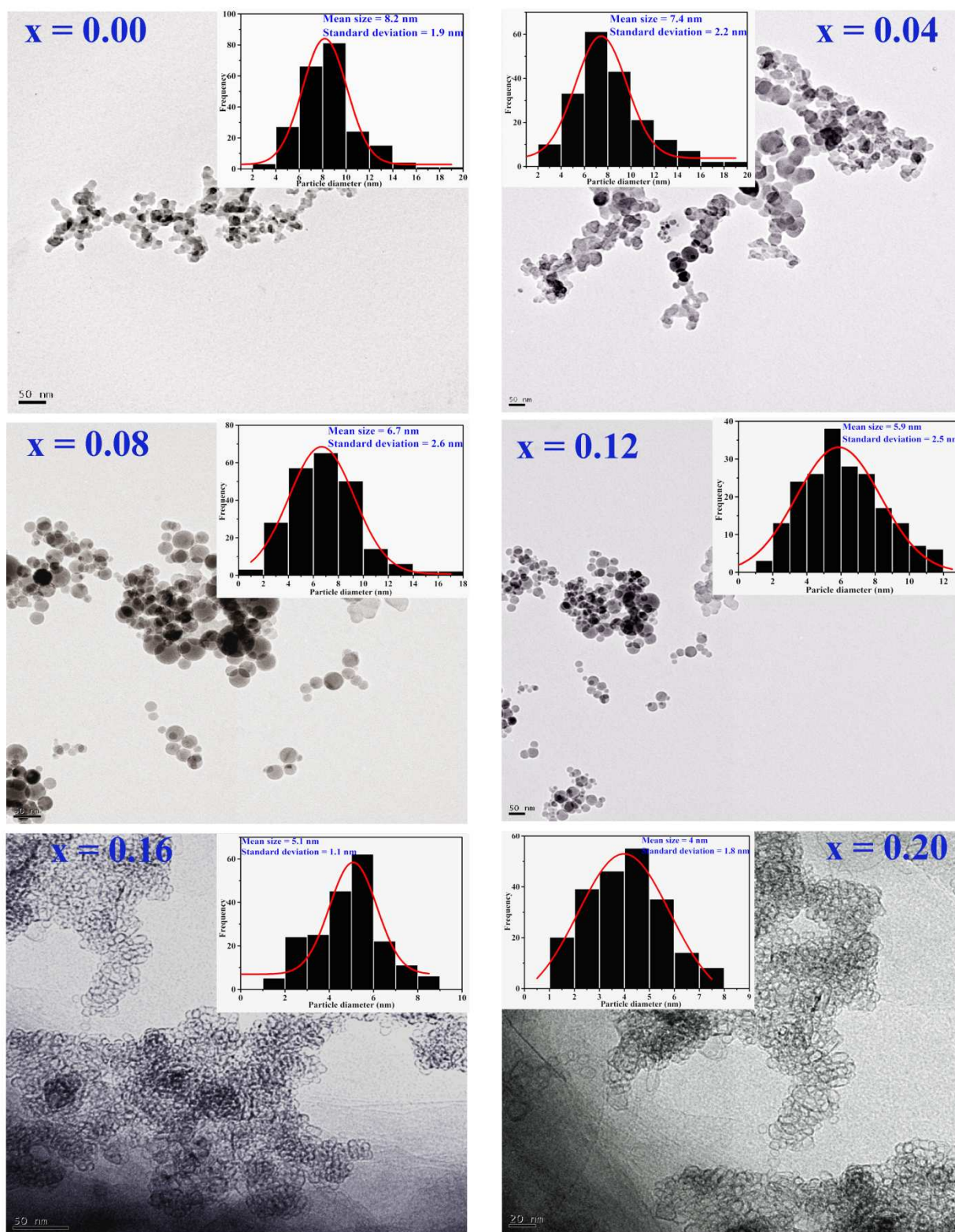

Fig.2 TEM images and number-frequency histograms of $Co_{1-x}Mg_xFe_2O_4$ powder annealed at 1050 °C. The solid line is a Gaussian fit.

The estimated average particle size has been observed to decrease gradually from 8.2 to 4.0 nm with increasing magnesium content and such behaviour was reported, earlier in $Ni_{0.5}Cu_{0.05}Mg_xZn_{0.45-x}Fe_2O_4$, $Mg_xZn_{1-x}Fe_2O_4$ nano ferrite systems [22, 23]. The reason for the observed decrease could be due to the stable nature of the magnesium oxide which acts as a microstructural stabilizer in avoiding the occurrence of divalent iron and becomes responsible for the finer and uniform grain growth. Moreover, the decrease of particle size may also be due to increase in porosity since the pores neutralize the driving force and leading to the increase in thickness of the grain boundary. The observed microstructural change in terms of increase in porosity with a decrease in grain size has been evident in FESEM micrographs of the samples (figure 3).
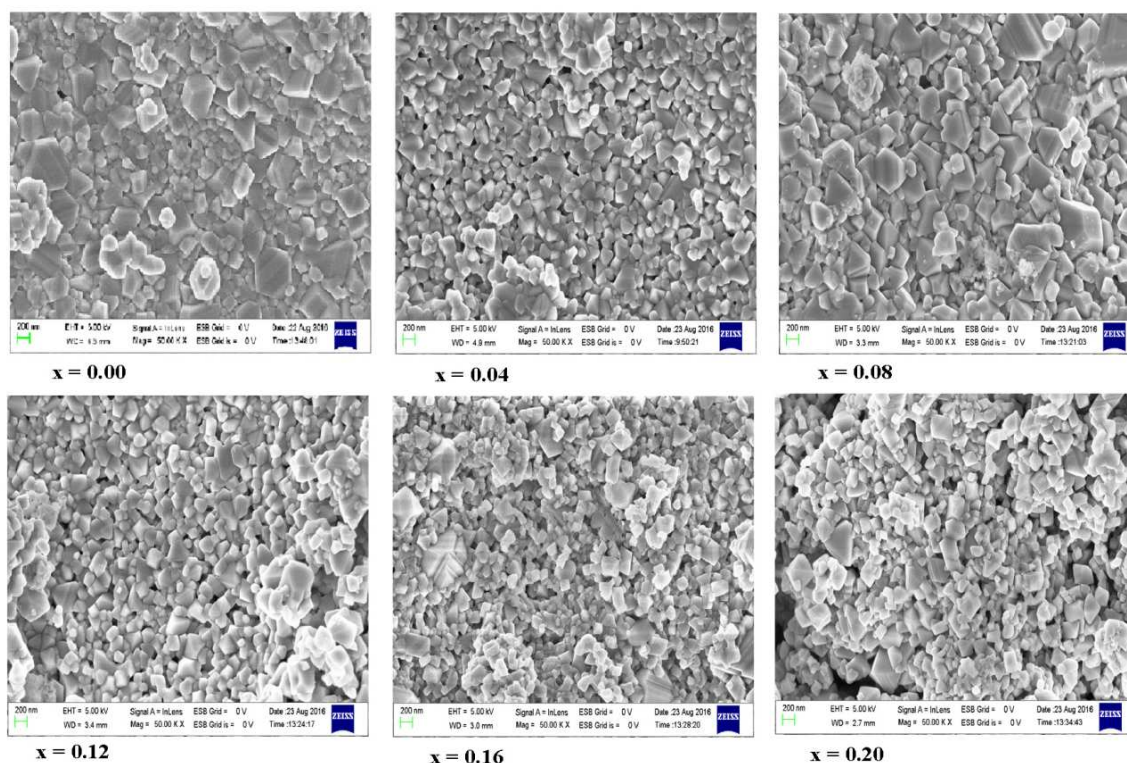

Fig.3 FESEM images of $Co_{1-x}Mg_xFe_2O_4$ pellets sintered at 1050 °C

Table 1 Lattice parameter, particle size, bulk density, X-ray density and percentage of porosity of $Co_{1-x}Mg_xFe_2O_4$ ferrite nanoparticles

x in $Co_{1-x}Mg_xFe_2O_4$	Lattice parameter (Å)	Particle size (TEM) (nm)	Bulk density (g/cm^3)	X-ray density (g/cm^3)	Percentage of porosity
0.00	8.3853	8.2	4.191	5.289	20.8
0.04	8.3801	7.4	4.161	5.262	20.9
0.08	8.3773	6.7	4.119	5.241	21.4
0.12	8.3740	5.9	4.087	5.218	21.7
0.16	8.3707	5.1	4.054	5.200	22.1
0.20	8.3680	4.0	4.019	5.179	22.4

3.3 Fourier transform Infrared spectra

The room temperature FTIR spectra of pure cobalt ferrite and magnesium substituted cobalt ferrites are shown in figures 4 and 5 respectively. The high frequency (υ_1) bands near 580 – 592 cm^{-1}and the lower frequency (υ_2) bands near 382-391 cm^{-1}correspond to the intrinsic lattice vibration of the tetrahedral group complexes Fe^{3+}- O^{2-} and octahedral group complexes Fe^{3+} - O^{2-} respectively. The band positions correspond to tetrahedral and octahedral metal complexes are presented in Table 2.
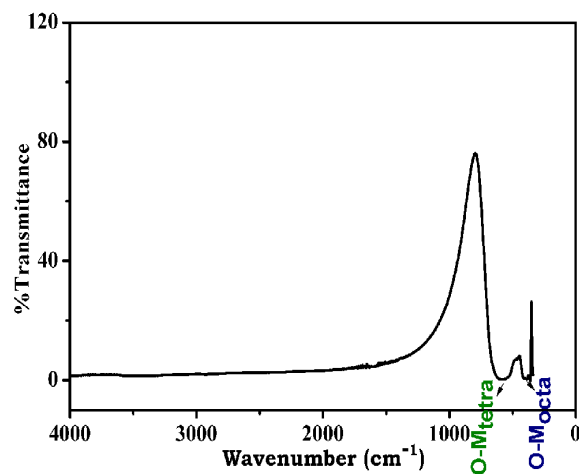

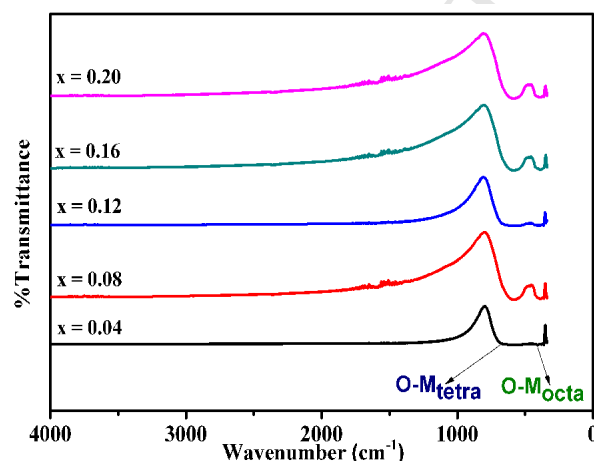*Fig.4 FT IR spectrum of cobalt ferrite*　　　　*Fig.5 FTIR spectra of Co$_{1-x}$Mg$_x$Fe$_2$O$_4$*

Table 2 Band positions and force constants for magnesium substituted cobalt ferrite

x in Co$_{1-x}$Mg$_x$Fe$_2$O$_4$	ν_1 (tetrahedral) (cm^{-1})	ν_2 (octahedral) (cm^{-1})	Fe^{3+} - O^{2-} bond force constant (10^5 dyne/cm)	
			Tetrahedral (K_T)	Octahedral (K_O)
0.00	580	382	2.38	1.10
0.04	583	383	2.41	1.10
0.08	586	385	2.45	1.11
0.12	588	388	2.47	1.13
0.16	590	389	2.49	1.13
0.20	592	391	2.52	1.14

The tetrahedral band (υ_1) and octahedral band (υ_2) are observed to shift towards the higher wave numbers with the magnesium concentration and the shift in the octahedral band (υ_2) indicates Mg^{2+} ions prefer to occupy octahedral sites and push Fe^{3+} ions towards oxygen ions by which the distance between Fe^{3+} - O^{2-} decreases due to its larger ionic radius than Fe^{3+} (0.645 Å) ion. Similar finding was reported in Mg substituted NiCuZn ferrites prepared through sol-gel method by Sujatha et al. [22]. The observed less intense band near 416 cm^{-1} (figure 6) reveals the presence of divalent magnesium ions at octahedral sites corresponding to the Mg^{2+} - O^{2-} octahedral complexes [16]. The shift of the tetrahedral absorption band is

due to change in bond length at A-sites, causing an increase in force constant of the tetrahedral site with the substitution of magnesium ions. The force constant for the bond Fe^{3+} - O^{2-} has been calculated from the equation [24] $K = 4\pi^2 c^2 \nu^2 \mu$, where c is the speed of light, ν is the wave number of bands in cm^{-1} and μ is the reduced mass for Fe^{3+} and O^{2-} ions. The force constant, thus estimated for the tetrahedral site increases from 2.38 x 10^5 to 2.52 x 10^5 dyne/cm. In general, the decrease in bond length, and increase in force constant for either site may be expected if the radius of the impurity ion is smaller than the displaced ion. The magnesium ions occupy completely B-sites and force the Fe^{3+} ions at B-site to occupy tetrahedral sites. Fe^{3+} (lower atomic mass) ions, thus shifted replace the Co^{2+} ions at tetrahedral sites. In other words, the magnesium ions indirectly replace the cobalt ions at A-site and the weak band   362 cm^{-1}(figure 6) suggests the presence of cobalt divalent ions at the octahedral sites. The decrease in reduced mass and the displacement mechanism of Co^{2+} ion (0.58 Å) at tetrahedral sites with Fe^{3+} (0.49 Å) ion of smaller radius are responsible for the observed variation in band position and force constant.
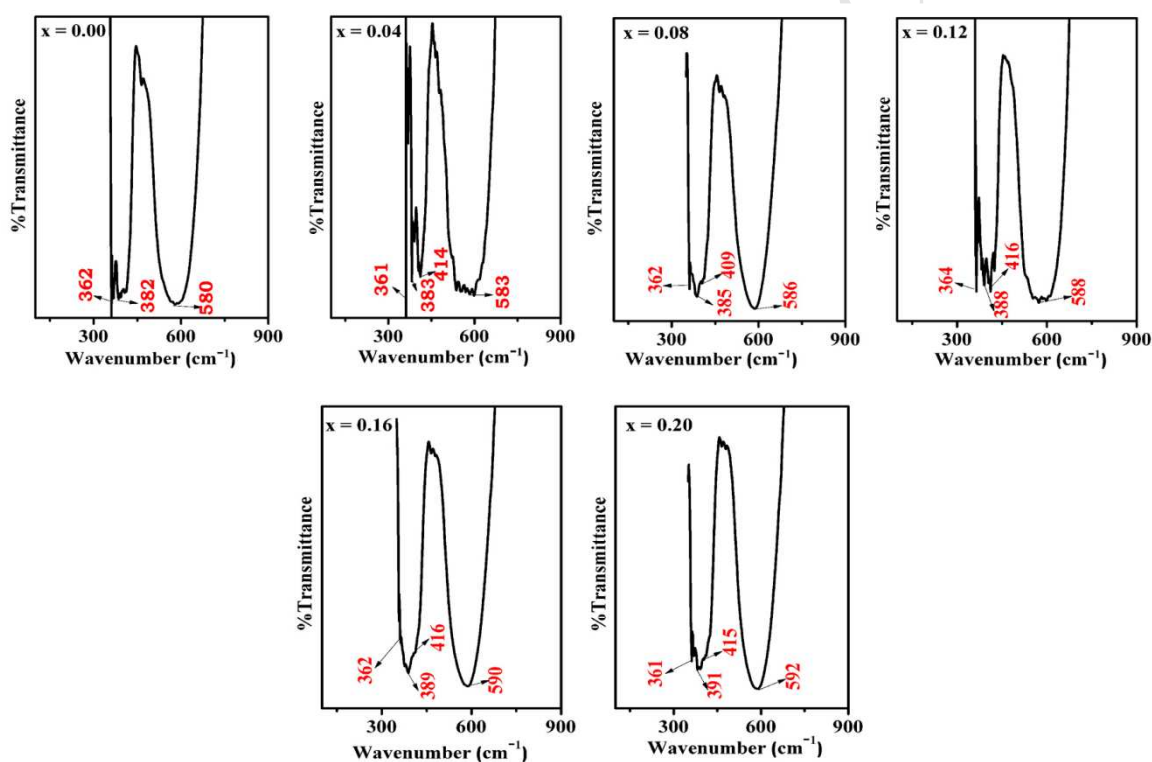

Fig.6 Magnified pictures of absorption bands of $Co_{1-x}Mg_xFe_2O_4$

3.4   Magnetic properties

Room temperature hysteresis loops for magnesium substituted cobalt ferrite samples are shown in figure 7. An overall decrease in the specific saturation magnetization (84.6 - 67.1 emu/g) has been noticed with increasing magnesium concentration (table 3). It is a well-known fact [25] that A–B exchange interaction in cobalt ferrite is predominant because nearly 20% cobalt resides on A-site. According to Neel model, A-B exchange interaction in ferrites is stronger and effective than A-A and B-B super exchange interactions and the net magnetic moment of the ferrite lattice is equal to the difference between the magnetic moments of A and B sublattices, i.e. $M = M_B - M_A$.
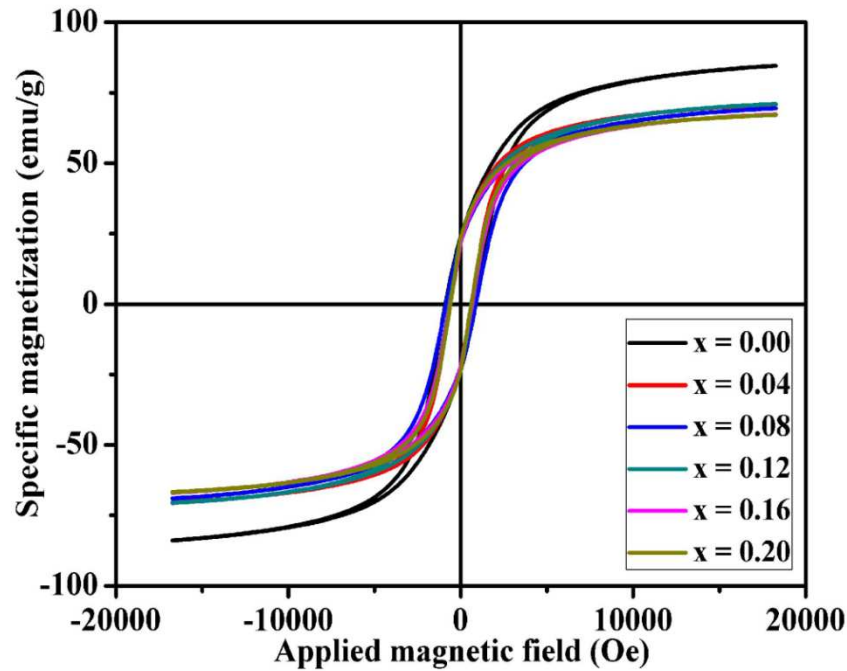
Fig.7 Room temperature hysteresis loops of $Co_{1-x}Mg_xFe_2O_4$.

As said in the previous section, magnesium ion substitution reduces the B-site magnetic moment by $5\mu_B$ and increases the A-site magnetic moment by $2\mu_B$. With increasing magnesium concentration, the B-site magnetic moment may closely approach the A-site magnetic moment provided the A-B exchange interaction is strong, leading to the net decrease of saturation magnetization. The observed decrease can further be supported considering the effects of magneto-crystalline anisotropy constant and Curie temperature with the increase in magnesium content.

The magneto-crystalline anisotropy constant (K) has been estimated using the relation [6],

$$K = \frac{M_s \times H_C}{0.96},$$

where Hc is coercive field, Ms is the maximum value of magnetization measured at 18 kOe applied magnetic field. The anisotropy constant is found to decrease gradually from $4.11 \times 10^6 erg/cm^3$ to $2.08 \times 10^6 erg/cm^3$ (table 3) with the increasing magnesium concentration. As is known, the magnetic anisotropy in non-cobalt containing ferrites arises from the Fe^{3+} ions present at the B-sub lattices whereas, in cobalt containing ferrites, a very large magnetic anisotropy arises primarily due to the presence of cobalt ions at B-sites [26]. The contribution to the magnetic anisotropy from divalent cobalt ions on the octahedral site through trigonal distortion is more than that of the ions present at the tetrahedral site.

Based on the discussion given in section 3.3, magnesium substitution in cobalt ferrite causes depletion of Fe^{3+} ions at B-site and increases the same at A-site. With the incorporation of magnesium, the amount of cobalt at A-site decreases continuously with no change in the cobalt content at B-site throughout the concentration studied. As the magnetic anisotropy contribution of divalent magnesium at octahedral site is less, the magnetic anisotropy of the ferrite system gradually decreases with increasing magnesium concentration [27]. The magnetic anisotropy values in nanoparticles are, in general higher than those reported for bulk cobalt ($1.8 \times 10^6 erg/cm^3$) and magnesium ($-3.75 \times 10^4 erg/cm^3$) ferrites [28] and as expected for nano sized particles, the high surface anisotropy plays a fundamental role in increasing the total anisotropy of the nanoparticles [18].

Table 3 Magnetic properties and activation energy for magnesium substituted cobalt ferrite

x in $Co_{1-x}Mg_xFe_2O_4$	Specific Saturation magnetization (emu/g)	Coercivity (Oe)	Anisotropy constant (10^6 erg/cm^3)	Curie temperature (°C)	Activation energy (eV)
0.00	84.6	885	4.11	476	0.67
0.04	70.8	640	2.47	468	0.68
0.08	69.5	875	3.28	460	0.71
0.12	71.0	673	2.56	455	0.72
0.16	67.3	634	2.26	450	0.85
0.20	67.1	590	2.08	446	0.96

The Curie temperature, measured from the temperature dependence of initial permeability (μ_i) in the temperature range 40°C – 540°C for all the magnesium substituted cobalt ferrite samples at a constant frequency 100 kHz is shown in figure 8. An abrupt drop in initial permeability near the Curie point indicates a good compositional homogeneity in all the samples and the absence of secondary maximum in μ_i versus T graph indicates the formation of single phase ferrite samples as shown by XRD patterns.
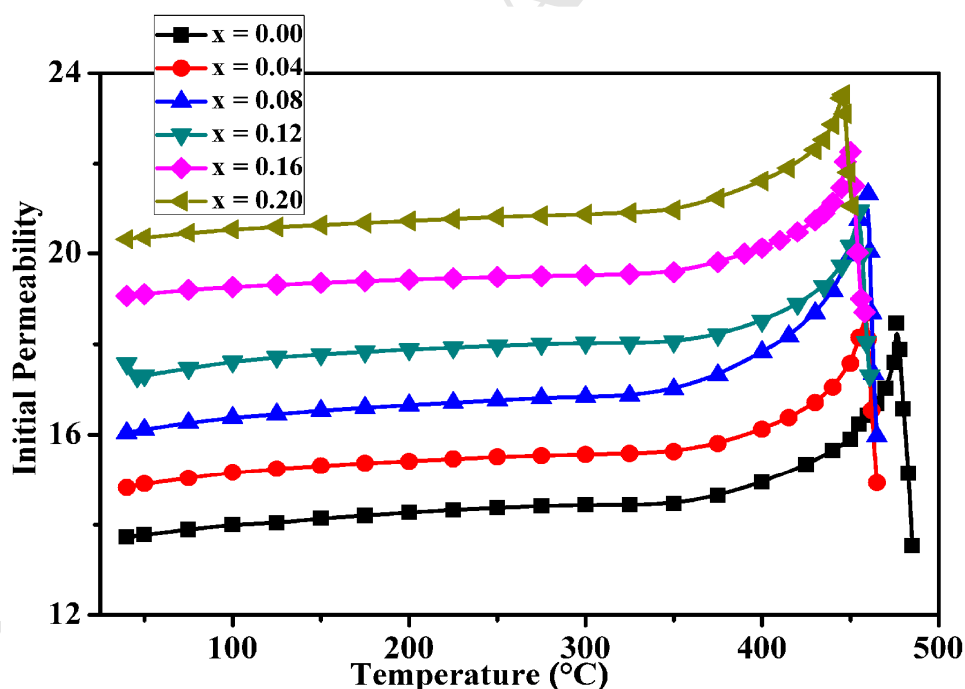

Fig.8 Variation of initial permeability with temperature in Co$_{1-x}$Mg$_x$Fe$_2$O$_4$

The observed decrease (table 3) in Curie temperature can be explained based on the exchange interactions and the site occupancy of magnesium ions. From the discussion made in an earlier section, the incorporation of diamagnetic magnesium in place of cobalt transfers Fe^{3+} ions from B to A site and decreases the density of magnetic ions at those sites. The process not only reduces the magnetic moment of the B-sub lattice, but also A-B exchange interaction which is reflected in the fall of Curie temperature with the increasing magnesium

concentration. The fall of Curie temperature, associated with the replacement of magnetic ions by diamagnetic ions has been a well-known phenomenon [25, 29].

3.5   DC resistivity

The variation of DC resistivity as a function of temperature is shown in figure 9. As expected in semiconductors, the resistivity of all the ferrite samples has been observed to decrease exponentially with the increasing temperature. The increase in resistivity at lower temperature below 400K was ascribed [30, 31] to the impurities present in the sample, which become negligible at higher temperatures. Hence, the resistivity has been measured in the temperature above 400K for all the samples.

The variation of DC resistivity measured at 120°C as a function of magnesium concentration is shown in figure 10. The observed increase throughout the concentration studied can be explained based on Verwey mechanism [32]. According to Verwey, the electronic conduction in ferrites is primarily due to hopping of electrons between the ions of the same element present in more than one valance state. In ferrite crystalline structure, the distance between two metal ions present at B-sites is smaller than the distance between a metal ion at B-site and another metal ion at A-site. The electron hopping between ions residing at B and A sites under normal conditions, therefore, has a very small probability as compared to that of hopping between ions at B–B sites. Hopping between ions at A–A sites will not take place for the simple reason that Fe^{2+} ions prefer to occupy B-sites only.

The observed grain size, in the present investigation is less than that reported by other researchers on the same composition [16, 17]. Smaller the grain size, the larger the number of grain boundaries, causing higher values of DC resistivity in the material. In the basic composition (x = 0.00), a small amount of Fe^{2+} content might be expected due to higher annealing temperature. As mentioned earlier, substituted magnesium in place of cobalt occupies the B-site and transfers an equal amount of Fe^{3+} ions from B-site to A-site, which replaces Co^{2+} ions present at A- sites. The amount of Fe^{3+} ions available at B-sites will be exhausted gradually with increasing concentration of magnesium. Thus, hopping probability between ions of different valence states available at B-sites will be reduced and consequently the DC resistivity increases with the concentration of magnesium.

The plots of log ρ versus 1/T are shown in figure 11. The activation energies, determined from the slopes of these curves increase gradually from 0.67 to 0.96eV (table 3) with the magnesium concentration. Activation energy for electron hopping in ferrites was reported to be around 0.4eV [33]. The higher values recorded in the present study suggest the conduction mechanism could be due to polaron hopping. Similar inference for higher values of activation energy was provided by several researchers [34, 35]. The probability for hopping mechanism is connected with the energy barrier, encountered by the electrons during hopping besides the size of the grain. Bigger grains with increased grain to grain contact area lower the barrier height and promote the process of hopping [36] whereas, in the present work, reduced grain size with magnesium concentration enhances the energy barrier height which reflects in higher activation energy values with magnesium concentration.
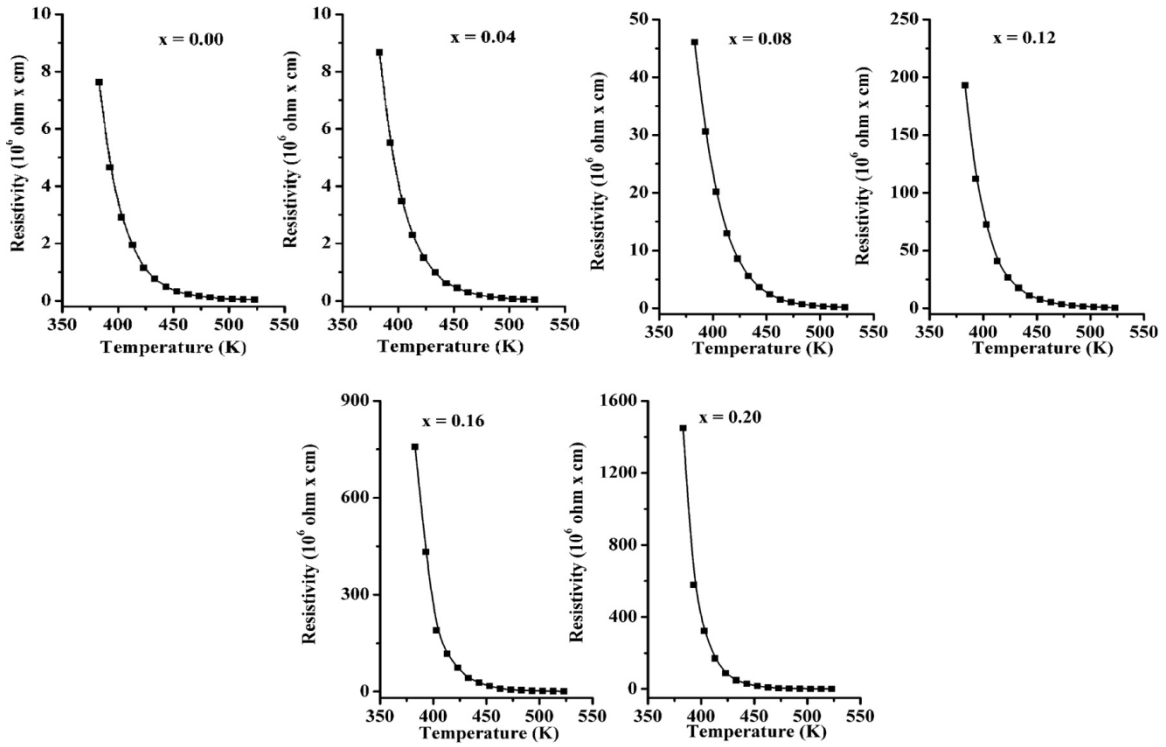
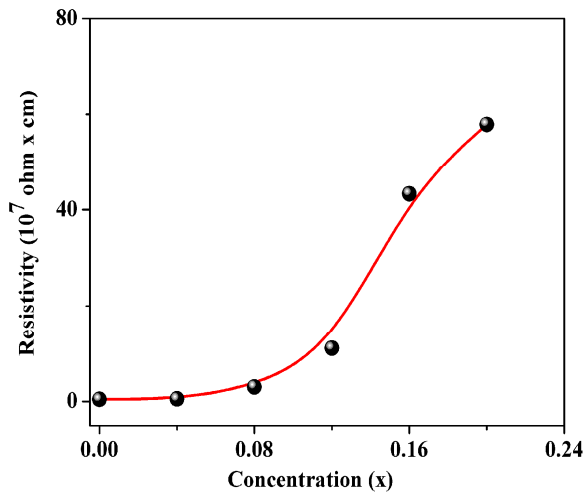*Fig.9 Variation of DC resistivity with temperature in Co$_{1-x}$Mg$_x$Fe$_2$O$_4$*

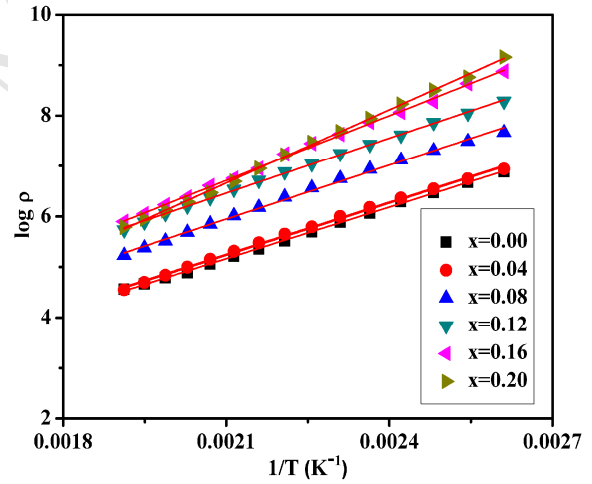*Fig.10 DC resistivity as a function of magnesium concentration.*

Fig.11 logρ versus 1/T plots

3.6 Cation distribution

Based on the preferences of various metallic ions and the above discussion, the cation distribution for the series of samples has been proposed and given in the table 4. Further, to check the correctness of the proposed distributions, lattice constant (a) has been calculated for each composition using the proposed distribution and some needy mathematical formulae as given below [37];

$$a_{\text{Calculated}} = \frac{8}{3\sqrt{3}}\left[\left(r_A + R_0\right) + \sqrt{3}\left(r_B + R_0\right)\right]$$

where r_A and r_B are the mean radii of the tetrahedral and octahedral sites and R_o is the radius of oxygen ion. Shanon radii (radii of cations in respective sites) have been used in determining the lattice parameter.

Table 4 Proposed cationic distribution, calculated oxygen parameter and bond lengths of magnesium substituted cobalt ferrite

x in $Co_{1-x}Mg_xFe_2O_4$	Proposed cationic distribution	u	Bond length (Å)	
			Tetrahedral (d_{AO})	Octahedral (d_{BO})
0.00	$(Co_{0.20} Fe_{0.80}) [Co_{0.80} Fe_{1.20}] O_4$	0.382	1.874	2.063
0.04	$(Co_{0.16} Fe_{0.84}) [Co_{0.8} Mg_{0.04} Fe_{1.16}] O_4$	0.383	1.872	2.061
0.08	$(Co_{0.12} Fe_{0.88}) [Co_{0.80} Mg_{0.08} Fe_{1.12}] O_4$	0.385	1.871	2.060
0.12	$(Co_{0.08} Fe_{0.92}) [Co_{0.80} Mg_{0.12} Fe_{1.08}] O_4$	0.388	1.870	2.059
0.16	$(Co_{0.04} Fe_{0.96}) [Co_{0.80} Mg_{0.16} Fe_{1.04}] O_4$	0.389	1.869	2.058
0.20	$(Fe) [Co_{0.80} Mg_{0.20} Fe] O_4$	0.391	1.868	2.057

The values of r_A and r_B can be calculated using the equations given below,

$$r_A = (0.2 - x) r_{Co} + (0.8 + x) r_{Fe}$$

$$\text{and } r_B = \frac{1}{2}\left[0.8 r_{Co} + x r_{Mg} + (1.2 - x) r_{Fe}\right]$$

The close agreement between the calculated and experimental lattice parameters (figure 12) supports that the site occupancy of magnesium ions at octahedral sites and the proposed distributions are correct.

The oxygen parameter (u) was calculated using the relation $u = \left[(r_A + R_0)\frac{1}{\sqrt{3}\ a} + \frac{1}{4}\right]$, where a is the calculated lattice parameter, R_0 is the radius of oxygen ion (1.37Å), and r_A is the tetrahedral ionic radius [37]. The calculated values, shown in the table 4 are very close to that reported value (0.375) in the spinel structure.

Tetrahedral and octahedral bond lengths (d_{AO} & d_{BO}) in a unit cell of spinel lattice have also been estimated using the following relations [38], $d_{AO} = a\sqrt{3}(u - 0.25)$, $d_{BO} = a\left(3u^2 - \frac{11}{4}u + \frac{43}{64}\right)^{\frac{1}{2}}$ where a is the calculated lattice parameter and u is the calculated oxygen parameter. The observed contraction in Fe^{3+} - O^{2-} bond lengths at both the tetrahedral and octahedral sites has been reflected in showing the decreasing trend in lattice parameter, besides the shifting of the tetrahedral, octahedral bands towards higher frequencies and the respective increase in force constants in sites with magnesium concentration. The reduction in tetrahedral and octahedral bond lengths, particle size, saturation magnetization, and close agreement between experimental and calculated lattice parameters lead to a conclusion that magnesium ions occupy B sites.
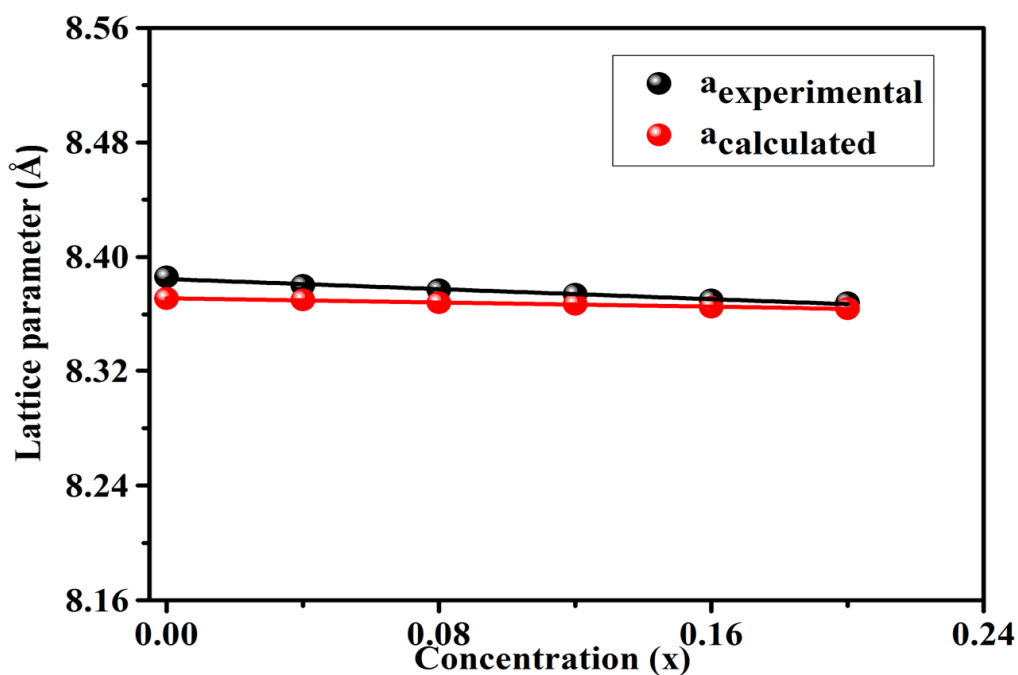
Fig.12. Variation of lattice parameter (a_{exp} and a_{cal}) with magnesium concentration.

4. Conclusion

The sol-gel method has been proved to be very effective in producing the particles of smaller sizes coupled with reasonably high saturation magnetization throughout the magnesium concentration studied. The study establishes the occupancy of magnesium ions at octahedral sites. The reduced values of coercivity, magnetic anisotropy, and Curie temperature are agreeable with the required characteristics of materials useful for biomedical applications.

5. Acknowledgements

References

[1]   I. C. Nlebedim, N. Ranvah, Y. Melikhov, P. I. Williams, J. E. Snyder, A. J. Moses, and D. C. Jiles, Effect of temperature variation on the magnetostrictive properties of $CoAl_xFe_{2-x}O_4$, J. Appl. Phys. 107, 09A936 (2010).

[2]   Jean-Paul Fortin, Claire Wilhelm, Jacques Servais, Christine Ménager, Jean-Claude Bacri, and Florence Gazeau,Size-Sorted Anionic Iron Oxide Nanomagnets as Colloidal Mediators for Magnetic Hyperthermia, J. Am. Che. Soc 129 (*2007) 2628-2635.

[3]   Elvira Fantechi, Claudia Innocenti, Martin Albino, Elisabetta Lottini and Claudio Sangregorio, Influence of cobalt doping on the hyperthermic efficiency of magnetite nanoparticles, J. Magn. Magn. Mater. 380 (2015) 365-371.

[4]   E. L. Verde, G. T. Landi, J. A. Gomes, M. H. Sousa, and A. F. Bakuzis, Magnetic hyperthermia investigation of cobalt ferrite nanoparticles: Comparison between experiment, linear response theory, and dynamic hysteresis simulations, J. Appl. Phys. 111 (2012)123902

[5]   Muvvala Krishna Surendra, Rajesh Dutta and M S Ramachandra Rao, Realization of highest specific absorption rate nearsuperparamagnetic limit of $CoFe_2O_4$ colloids for magnetic hyperthermia applications, Materials Research Express 1 (2014) 026107

[6]   K.Srinivasa Rao, S.V.Ranga Nayakulu, M.Chaitanya Varma, G.S.V.R.K.Choudary and K.H.Rao, Controlled phase evolution and the occurrence of single domain $CoFe_2O_4$ nanoparticles synthesized by PVA assisted sol-gel method, J. Magn. Magn. Mater. 451 (2018) 602-608.

[7]   B.G.Toksha, Sagar E, Shirsath, S.M.Patange and K.M.Jadhav,Structural investigations and magnetic properties of cobalt ferrite nanoparticles prepared by sol-gel auto combustion method, Solid State Commun. 147 (2008) 479-483.

[8]   Jae-Gwamg Lee, Jae Yun Park and Chul Sung Kim, Growth of ultra-fine cobalt ferrite particles by a sol–gel method and their magnetic properties, J. Mater. Sci. 33 (1998) 3965-3968.

[9]   Sonal singhal, Sheenu Jauhar, Jagdish Singh, Kailash Chandra and Sandeep Bansal, Investigation of structural, magnetic, electrical and optical properties of chromium substituted cobalt ferrites ($CoCr_xFe_{2-x}O_4$, $0 \leqslant x \leqslant 1$) synthesized using sol gel auto combustion method, J. Mol. Struct. 1012 (2012) 182-188.

[10]   Mukta V. Limaye, Shashi B. Singh, Sadgopal K. Date, Deepti Kothari, V. Raghavendra Reddy, Ajay Gupta, Vasant Sathe, Ram Jane Choudary and Sulabha K. Kulkarni,High Coercivity of Oleic Acid Capped $CoFe_2O_4$ Nanoparticles at Room Temperature, J. Phys. Chem. B 113 (2009) 9070-9076.

[11]   A.V. Raut, R.S. Barkule, D.R. Shengule and K.M. Jadhav, Synthesis, Structural investigation and magnetic properties of Zn2+ substituted cobalt ferrite nanoparticles prepared by the sol-gel auto-combustion technique, J. Magn. Magn. Mater. 358-359 (2014) 87-92.

[12]   Sonal Singhal, Tsering Namgyal, Sandeep Bansal and Kailash Chandra, Effect of Zn Substitution on the Magnetic Properties of Cobalt Ferrite Nano Particles Prepared Via Sol-Gel Route, J. Electromagnetic Analysis & Applications 2 (2010) 376-381

[13]   Julia Mürbe and Jörg Töpfer, Phase Formation, Sintering Behavior, and Magnetic Properties of Low-Temperature Fired Mg-Cu-Zn Ferrites, J. Am. Ceram. Soc. 95 (2012) 3883–3888.

[14]   Muddassar Naeem, Nazar Abbas Shah, Iftikhar Hussain Gul and Asghari Maqsood, Structural, electrical and magnetic characterization of Ni-Mg spinel ferrites, J. Alloys Compd. 487 (2009) 739–743.

[15]   Li Wang, Ming Lu, Yu Liu, Ji Li, Mei Liu and Haibo Li, The structure, magnetic properties and cation distribution of $Co_{1-x}Mg_xFe_2O_4/SiO_2$ nanocomposites synthesized by sol–gel method, Ceram. Int. 41(2015)4176-4181.

[16]   Tulu Wegayehu Mammo, N, Murali, Yonatan Mulushoa Sileshi and T. Arunamani, Studies of structural, morphological, electrical, and magnetic properties of Mg-substituted Co-ferrite materials synthesized using sol-gel autocombustion method, Physica B 523 (2017) 24-30

[17]   H.S. Mund and B.L. Ahuja, Structural and magnetic properties of Mg doped cobalt ferrite nanoparticles prepared by sol-gel method, Mater. Res. Bull. 85 (2017) 228–233

[18]   A. Franco Jr., F. C.Silva and Vivien S. Zapf, High temperature magnetic properties of $Co_{1-x}Mg_xFe_2O_4$ nanoparticlesprepared by forced hydrolysis method, J. Appl. Phys. 111(2012) 07B530

[19] Vithal Vinayak, Pankaj P. Khirade, Shankar D. Birajdar, D. B. Sable and K. M. Jadhav, Structural, Microstructural, and Magnetic Studies on Magnesium (Mg^{2+})-Substituted $CoFe_2O_4$ Nanoparticles, J Supercond Nov Magn 29 (2016) 1025–1032

[20] H.S. Mund and B.L. Ahuja, Structural and magnetic properties of Mg doped cobalt ferrite nanoparticles prepared by sol-gel method, Mater. Res. Bull. 85 (2017) 228-233

[21] W.B. Dlamini, J.Z. Msomi and T. Moyo, XRD, Mössbauer and magnetic properties of $Mg_xCo_{1-x}Fe_2O_4$ nanoferrites , J. Magn. Magn. Mater.373(2015)78-82.

[22] Ch.Sujatha, K.Venugopal Reddy, K.Sowri Babu, A.Rama Chandra Reddy and K.H.Rao, Structural and magnetic properties of Mg substituted NiCuZn Nano Ferrites, Physica B: Condenced Matter. 407(2012)1232-1237.

[23] A Daigle, JModest, A L Geiler, S Gillette, YChen, MGeiler, B Hu, S Kim, K Stopher, C Vittoria1 and V G Harris, Structure, morphology and magnetic properties of $Mg_{(x)}Zn_{(1-x)}Fe_2O_4$ ferrites prepared by polyol and aqueous co-precipitation methods: a low-toxicity alternative to $Ni_{(x)}Zn_{(1-x)}Fe_2O_4$ ferrites, Nanotechnology 22 (2011) 305708 (6pp).

[24] P.A. Shaikh, R.C. Kambale, A.V. Rao and Y.D. Kolekar, Structural, magnetic and electrical properties of Co-Ni-Mn ferrites synthesized by co-precipitation method, J. Alloys Compd 492 (2010) 590-596.

[25] K. Srinivasa Rao, A. Mahesh Kumar, M. ChaitanyaVarma, G.S.V.R.K. Choudary and K.H. Rao, Cation distribution of titanium substituted cobalt ferrites, J. Alloys Compd. 488 (2009) L6–L9.

[26] Y.Mohammadifar, H.Shokrollahi, Z.Karimi and L.Karimi, The synthesis of $Co_{1-x}Dy_xFe_2O_4$ nanoparticles and thin films as well as investigating their magnetic and magneto-optical properties, J. Magn. Magn. Mater. 366(2014)44-49.

[27] I. C. Nlebedim, R. L. Hadimani, R. Prozorov and D. C. Jiles, Structural, magnetic, and magnetoelastic properties of magnesium substituted cobalt ferrite J. Appl. Phys. 113(2013)17A928.

[28] M. I. Darby and E. D. Isaac, Magnetocrystalline anisotropy of ferro- and ferrimagnetics, IEEE. Trans. Magn. 10(1974) 259-304.

[29] H.H.Joshi, P.B.Pandya, K.B.Modi, N.N.Jani, G.J.Baldha and R.G.Kulkarni, Magnetic properties of magnesium-cobalt ferrites synthesized by co-precipitation method, Bull. Mater. Sci 20(1997)93-101.

[30] P.P. Hankare, K.R. Sanadi, R.S. Pandav, N.M. Patil, K.M. Garadkar and I.S. Mulla, Structural, electrical and magnetic properties of cadmium substituted copper ferrite by sol–gel method, J. Alloys Compd. 540 (2012) 290 - 296.

[31] P.A. Shaikh, R.C. Kambale, A.V. Rao and Y.D. Kolekar, Studies on structural and electrical properties of $Co_{1-x}Ni_xFe_{1.9}Mn_{0.1}O_4$ ferrite, J. Alloys Compd. 482 (2009) 276 - 282.

[32] E.J.W. Verwey and J.H.De Boer, Cation arrangement in a few oxides with crystal structures of the spinel type, Rec. Trav. Chim. Pays Bas 55(1936)531-540.

[33] A.M.Abdeen, Dielectric behaviour in Ni–Zn ferrites, J. Magn. Magn. Mater. 192(1999)121-129.

[34] I.H. Gul, A.Z. Abbasi, F. Amin, M. Anis-ur-Rehman and A. Maqsood, Structural, magnetic and electrical properties of $Co_{1-x}Zn_xFe_2O_4$ synthesized by co-precipitation method, J. Magn. Magn. Mater. 311 (2007) 494–499

[35] Uday Bhasker Sontu, Vijaya kumar Yelasani and Venkata Ramana Reddy Musugu, Structural, electrical and magnetic characteristics of nickel substituted cobalt ferrite nano particles, synthesized by self combustion method, J. Magn. Magn. Mater. 374(2015)376–380.

[36]   I.H. Gul, F. Amin, A.Z. Abbasi, M. Anis-ur-Rehman and A. Maqsood, Physical and magnetic characterization of co-precipitated nanosize Co-Ni ferrites, Scr. Mater. 56 (2007) 497–500

[37]   M.A.Gabal and Y.M.Al Angari, Low-temperature synthesis of nanocrystalline NiCuZn ferrite and the effect of Cr substitution on its electrical properties, J. Magn. Magn. Mater. 322(2010)3159-3165.

[38]   Santosh Bhukal, Suman Mor, S.Bansal, Jagdish Singh and Sonal Singhal, Influence of Cd^{2+} ions on the structural, electrical, optical and magnetic properties of Co–Zn nanoferrites prepared by sol gel auto combustion method, J. Mol. Struct. 1071(2014)95-102.

Highlights

- Co-Mg ferrite nanoparticles with size 4.0-8.2 nm are synthesized by sol-gel method
- The chelating agent adequately controls the particle size
- High saturation magnetization has been achieved for these particles
- Magnetic properties have been discussed in terms of a proposed cation distribution
- The study establishes the occupancy of magnesium ions at octahedral sites.